Supplementary Material

Decoupling edge versus bulk conductance in the trivial regime of InAs/GaSb double quantum well using Corbino ring geometry.

Binh-Minh Nguyen*, Andrey A. Kiselev, Ramsey Noah, Wei Yi, Fanming Qu, Arjan J.A. Beukman, Folkert K. de Vries, Jasper van Veen, Stevan Nadj-Perge, Leo P. Kouwenhoven, Morten Kjaergaard, Henri J. Suominen, Fabrizio Nichele, Charles M. Marcus, Michael J Manfra, Marko Sokolich*

HRL Laboratories, 3011 Malibu Canyon Rd, Malibu, CA 90265, USA

QuTech and Kavli Institute of Nanoscience, Delft University of Technology, 2600 GA Delft, Netherlands

Center for Quantum Devices, Niels Bohr Institute, University of Copenhagen, 2100 Copenhagen, Denmark

Department of Physics and Astronomy, and Station Q Purdue, Purdue University, West Lafayette, Indiana 47907, USA

*Corresponding authors: mbnguyen@hrl.com and MSokolich@hrl.com

Contents

I. Evidence of trivial and inverted regimes in high mobility wafers

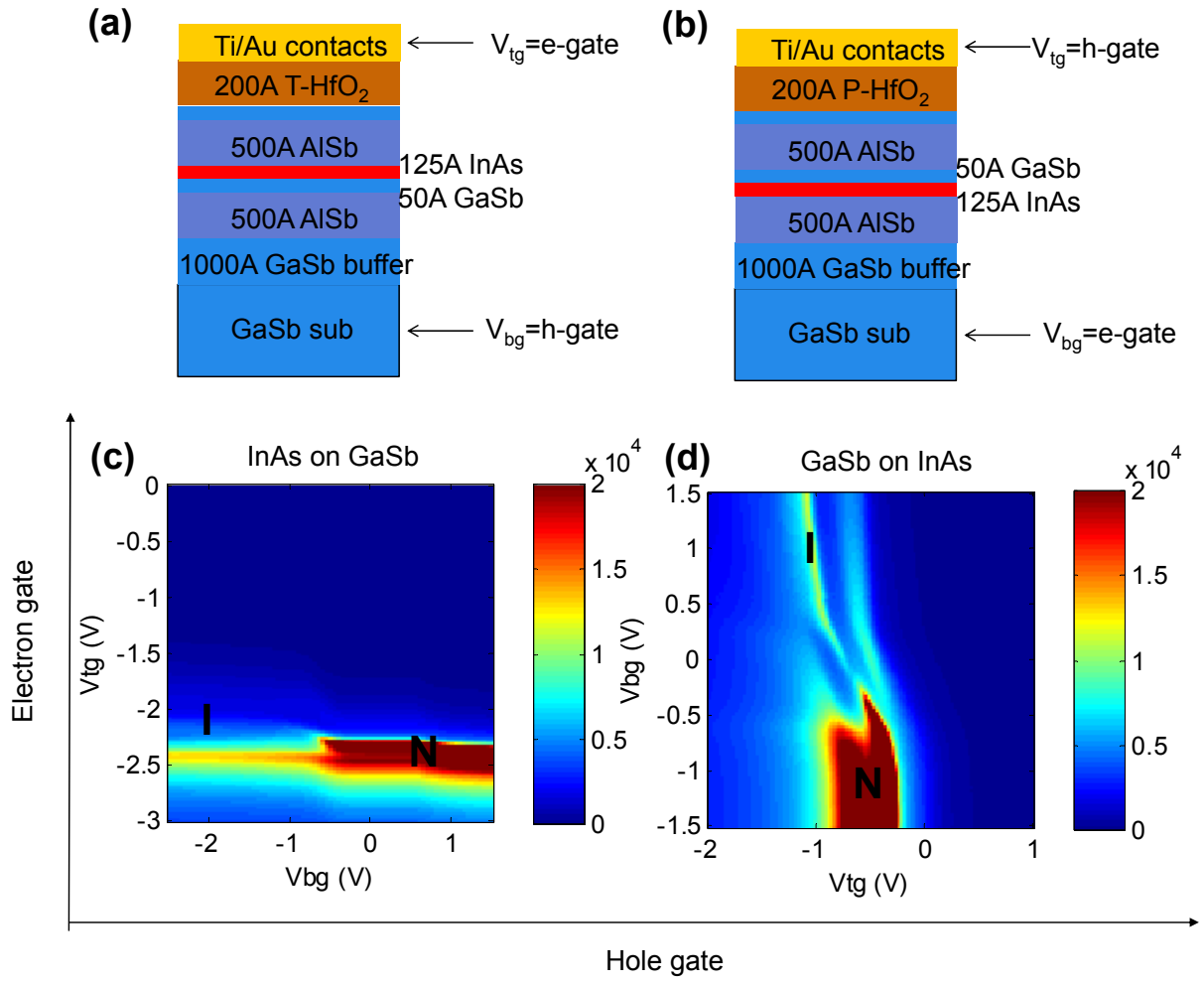

Figure S 1. *Device schematic and 2D phase diagram of high mobility wafers exhibiting a clear delineation between trivial and inverted regimes. (a,c) Wafer with InAs on GaSb sequencing similar to Ref 1 and Ref 2 and (b,d) Wafer with GaSb on InAs sequencing. All devices were processed using procedure reported in Ref. 1.*

II. Temperature dependence measurement and extraction

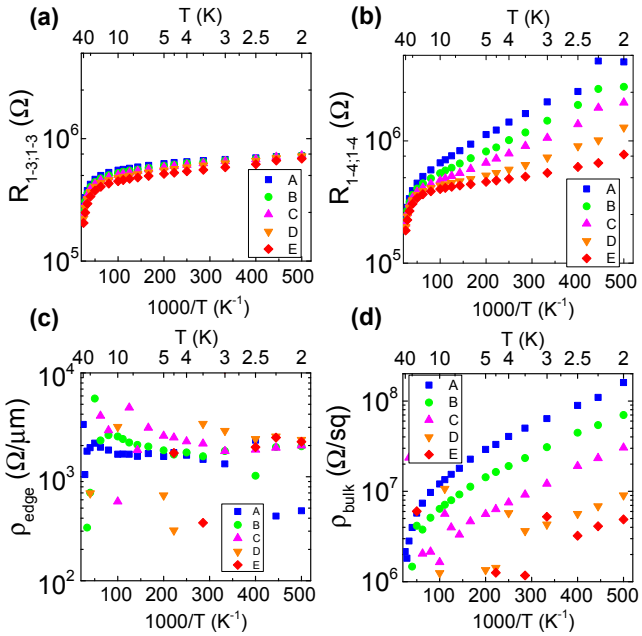

Figure S 2. Temperature dependence of (a) $R_{1\text{-}3;1\text{-}3}$ and (b) $R_{1\text{-}4;1\text{-}4}$, along with extracted values for (c) edge resistivity and (d) bulk resistivity at points A-E in Figure 1 (c), (d), main text. Edge resistivity and edge-dominated transport are temperature insensitive while bulk resistivity and bulk-dominated transport exhibit an Arrhenius trend with temperature.

As shown in Figure S 2 (a), (b), the temperature dependence of the RP peak resistance has two distinct regimes: below and above 10 K. Below 10 K, with edge contribution, the resistance is relatively insensitive to temperature while without edge, the resistance shows a clear dependence on temperature. Going from A to E, the trend is weakened, and eventually becomes temperature insensitive, which could be explained by a gapless scenario. Beyond point E, we did not see the gap reopening into the inverted regime, unlike previous high mobility devices (see Figure S 1 and Ref. *2*). The energy gap Δ was extracted from the Arrhenius trend $R \sim \exp(\Delta/2k_BT)$ to be ~13 K for point A and vanishing at E. At higher temperature regime (*T*>10 K), both resistances, with and without edges, roll over to a steeper slope, likely due to the fact that the bulk resistivity becomes so low that it now dominates the edge channel. The new energy gap is ~80 K, although reliable estimation is difficult. The

two-gap trend is similar to what was reported in Ref. [3] where the larger gap at high temperatures was assigned to be the hybridization-induced minigap and the smaller gap at low temperatures was assigned to be the localization gap. In Ref. [3], the transition between the two gap regimes also coincided with the turn on of the edge conductance, similar to what we see here in Figure S 2. However, in our case where the device was clearly in the trivial regime, the two energy gaps should not be due to the hybridization effect. Yet, its magnitude is conspicuously different from the expected direct gap between the conduction and valence states in the double layer. We speculate that a smaller gap could stem from disorder percolation[4] or from a localized shallow impurity level to either the conduction or valence band[5].

III. Extraction of bulk and edge resistivities

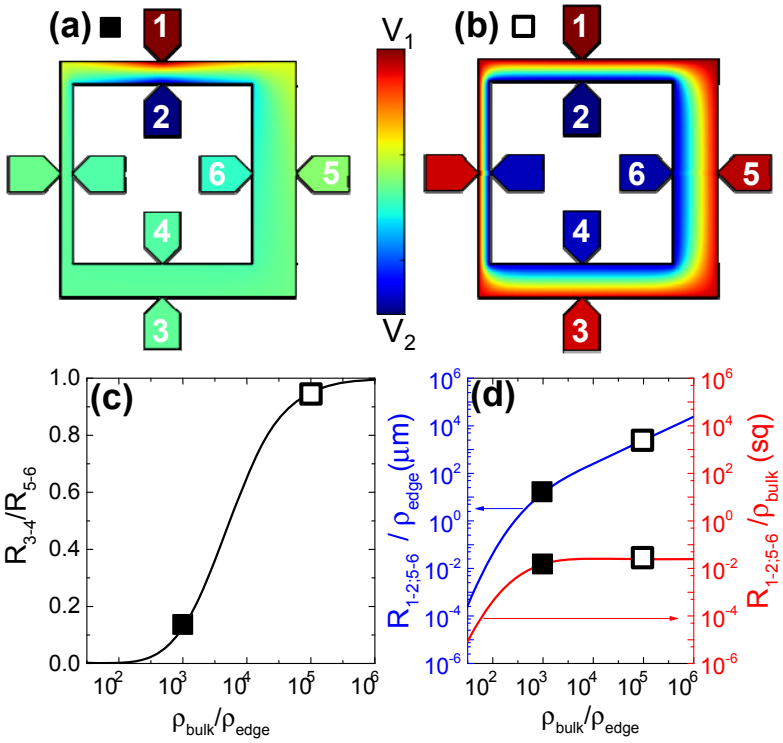

Figure S 3. Bias distribution maps simulated in the resistor network model for two cases of (a) modest (10^3) and (b) large (10^5) bulk-to-edge resistivity ratio; (c) resistance ratio $R_{1\text{-}2;3\text{-}4}/R_{1\text{-}2;5\text{-}6}$ and (d) scale

factors $R_{1\text{-}2;5\text{-}6}/\rho_{edge}$ and $R_{1\text{-}2;5\text{-}6}/\rho_{bulk}$ as a function of bulk-to-edge resistivity ratio. Markers ■ and □ in (c), (d) indicate the resistivity ratios used in the simulations depicted in (a) and (b), respectively. The arrows in (d) indicate the corresponding axis.

Shown in Figure S *3* (a) and (b) are bias distribution maps of our device when current is fed through terminals 1-2, for two representative ρ_{bulk}/ρ_{edge} ratios of 10^3 and 10^5 (μm per □). Smaller resistivity ratio means the bulk is relatively more conductive, leading to the current running straight in the mesa between terminals 1 and 2, while with larger resistivity ratio, the bulk becomes relatively more insulating, the lower resistance edges form quasi-equipotential contours extending around the whole device. This transition is exactly what we have observed in the experiment.

Beyond qualitative explanation of experimental data, the resistor network simulation also allows for a simultaneous extraction of edge and bulk resistivities. As shown in Figure S *3* (c), the resistance ratio $R_{1\text{-}2;\,3\text{-}4}/R_{1\text{-}2;5\text{-}6}$ is dictated by the ratio of bulk over edge resistivity alone, so the resistivity ratio can be extracted from the measured resistance ratio $R_{1\text{-}2;\,3\text{-}4}/R_{1\text{-}2;5\text{-}6}$ which does not involve contact resistance. Next, at a fixed ρ_{bulk}/ρ_{edge} ratio, the absolute resistance value $R_{1\text{-}2;5\text{-}6}$ scales linearly with the bulk (or, equivalently, edge) resistivity with a scale factor dependent on ρ_{bulk}/ρ_{edge}. Figure S *3* (d) plots the simulated ratio $R_{1\text{-}2;5\text{-}6}/\rho_{edge}$ (and also $R_{1\text{-}2;5\text{-}6}/\rho_{bulk}$, equal, of course, to $R_{1\text{-}2;5\text{-}6}/\rho_{edge}$ divided by ρ_{bulk}/ρ_{edge}) as a function of ρ_{bulk}/ρ_{edge}. This allows for independent evaluation of ρ_{edge} and ρ_{bulk} once $R_{1\text{-}2;5\text{-}6}$ and ρ_{bulk}/ρ_{edge} are determined.

To reflect chiral nature of edge channels at finite B (although with a possibility of closely spaced counter-propagating edge states that would allow some back scattering), we experimented also with simulations of a very similar and only minimally-modified *diode-resistor* network, which blocks (either fully or only partially) current backflow along the edges (with the preferable direction controlled by the sign of *B*). Thus, unlike the linear all-resistor network, the non-linear diode-resistor network is inherently sensitive

to the orientation of the applied magnetic field (or, equivalently, polarity of the feeding terminals), an observation of the model behavior that is fully supported by simulations. For the magnetic field pointing *into* the plane of the device in main text's Figure 1(b), current should prefer to flow clockwise along the outer edge of the device and counterclockwise along its inner edge. This is the case for the data measured at B=2 T shown in main text's Figure 2 (e)-(h). At high electron densities, i.e., deep in the IQHE regime, we simulate the experimental data using the *fully-blocking* diode-resistor network, while at the RP all-resistor network is more appropriate. For the lack of a detailed quantitative description of a crossover between these two regimes (where, intuitively, a partially-blocking diode-resistor network would be applicable), we attempted to simply patch them together along the crossover canyon boundary. Overall, the result is visually similar to the one obtained when processing data using the all-resistor network throughout [as depicted in main text's Figure 3 (c) and (d)]. Empirically, the edge in the diode-resistor network ends to be slightly more conductive (up to ~1.7x at largest ρ_{bulk}/ρ_{edge}) to compensate for the unidirectional current flow.

IV. Transport with-edge versus no-edge

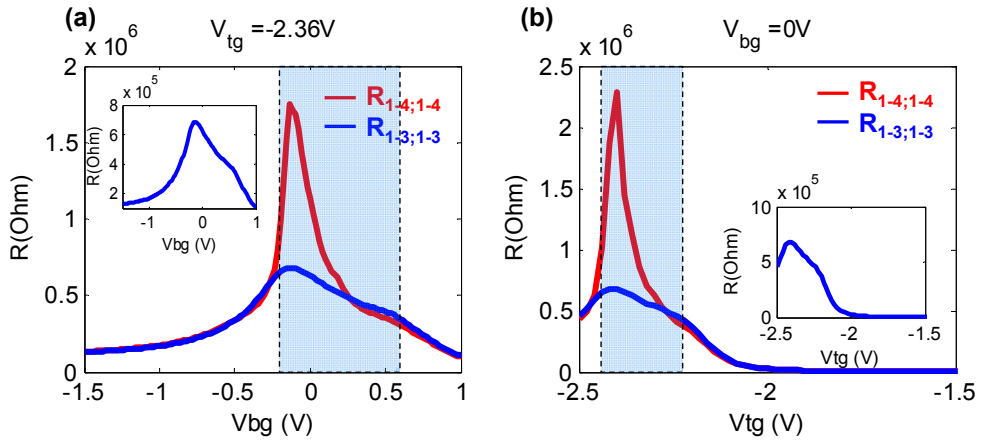

Figure S 4. 1D line cuts of $R_{1\text{-}3;1\text{-}3}$ and $R_{1\text{-}4;1\text{-}4}$ as a function of a) back gate bias at V_{tg}=-2.36 V and b) top gate bias at V_{bg}=0V. The on-set of edge conductance is indicated by the kinks of the $R_{1\text{-}3;1\text{-}3}$ curves, as well as by the deviation of $R_{1\text{-}3;1\text{-}3}$ from $R_{1\text{-}4;1\text{-}4}$ (dashed boxes). When dominated by edge conductance, the negative slope of the $R_{1\text{-}3;1\text{-}3}$ curves suggests an electron-nature of the edge transport. The peak of $R_{1\text{-}3;1\text{-}3}$ of 7 kΩ corresponds to an edge resistivity of 1.6 kΩ/μm for 2 parallel edge channels with length of 880 μm each. This edge resistivity is close to the extraction value of 2 kΩ/μm achieved with the resistor network model.

As discussed in the main text, the evidence of edge conductance can be seen from the comparison between $R_{1\text{-}3;1\text{-}3}$ (with edge)and $R_{1\text{-}4;1\text{-}4}$ (without edge). 1D line cuts of main text's Figure 1 (c) and (d) at a constant V_{tg}=-2.36 V and V_{bg}=0V are shown in Figure S 4 (a) and (b), respectively. When the bulk channel is highly conductive, there is no potential difference between leads 3 and 4 across the mesa, thus the two resistances overlap (outside of the dashed boxes). When the bulk becomes more resistive, leads 3 and 4 are electrically "disconnected", revealing a difference in conductance paths. Between leads 1 and 4, carrier must pass through the resistive bulk while between leads 1 and 3, carrier can travel along the edge if the bulk is too resistive. A deviation of $R_{1\text{-}3;1\text{-}3}$ from $R_{1\text{-}3;1\text{-}4}$ hence indicates the turn on of edge conductance.

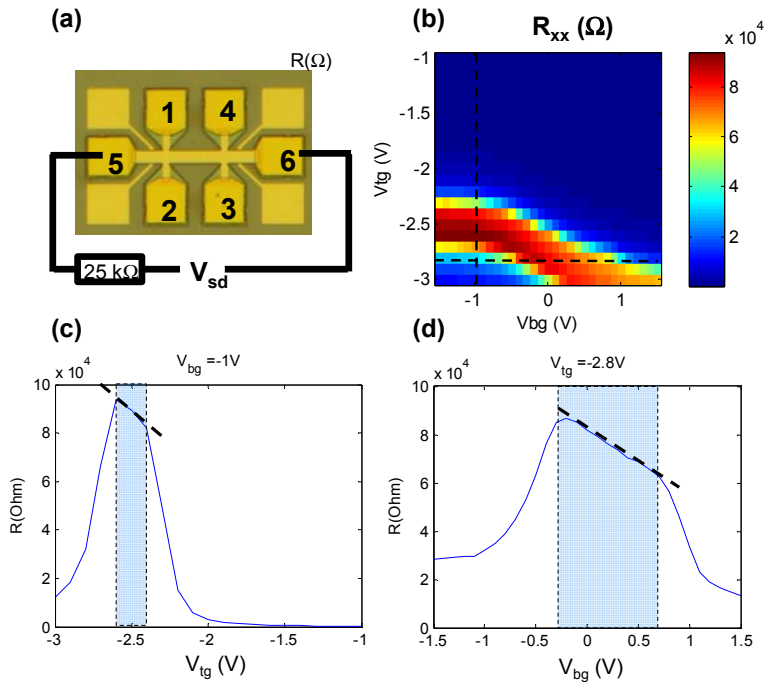

Figure S 5 (a) schematic of a Hall bar , (b) Longitudinal resistance ($R_{xx} = V_{23}/I_{56}$) map as a function of top and back gate biases, dashed lines indicate biases where a 1D line cut is plotted in (c) Vbg=-1V and (d) V_{tg}=-2.8V. Dashed boxes in (c) and (d) highlight edge-transport dominated regime. The negative slope of the resistance curve suggests an electron-nature of the edge transport. The resistance maxima of 94 kΩ scales with the edge length (100 μm for 2 parallel edges) with a linear edge resistivity scale factor of ~1.9 kΩ/μm. This edge resistivity is close to the extraction value of 2 kΩ/μm achieved with resistor network model.

Between leads 1 and 3, there are two possible parallel conductance path: (1) inside the bulk, along the mesa, and (2) at the outer edge of the mesa. The measured resistance is roughly the smaller between the two. When the bulk is more conductive than the edge (smaller resistance, outside of dashed boxes), the measured $R_{1\text{-}3;1\text{-}3}$ reflects the bulk resistance and when the bulk is more resistive than the edge (inside the dashed boxes), the measured $R_{1\text{-}3;1\text{-}3}$ reflects the edge resistance. The two kinks in $R_{1\text{-}3;1\text{-}3}$ curve right at the separation of $R_{1\text{-}3;1\text{-}3}$ and $R_{1\text{-}3;1\text{-}4}$ indicate a change in conductance mechanisms, which,

in this case, is the transition from bulk dominant to edge dominant conductance. The same kinked character is also observed in a Hall bar device with parallel edge-bulk channel (*Figure S 5*). Note that in the Hall bar, the longitudinal resistance R_{xx} does not involve contact resistance, so the kink-transition is not due to contact resistance effect. When dominated by the edge conductance, both $R_{1\text{-}3;1\text{-}3}$ of the Corbino ring and R_{xx} of the Hall bar have a decreasing trend with positive gate bias, suggesting an n-type nature of electron transport. Assuming the measured edge resistance is linear with length, we estimate the resistivity per unit length of 1.6 kΩ/μm and 2 kΩ/μm for the Corbino ring and Hall bar, respectively. These values are close to the ~2 kΩ/μm range numerically extracted from $R_{1\text{-}2;3\text{-}4}$ and $R_{1\text{-}2;5\text{-}6}$ data.

V. Local versus non-local measurement

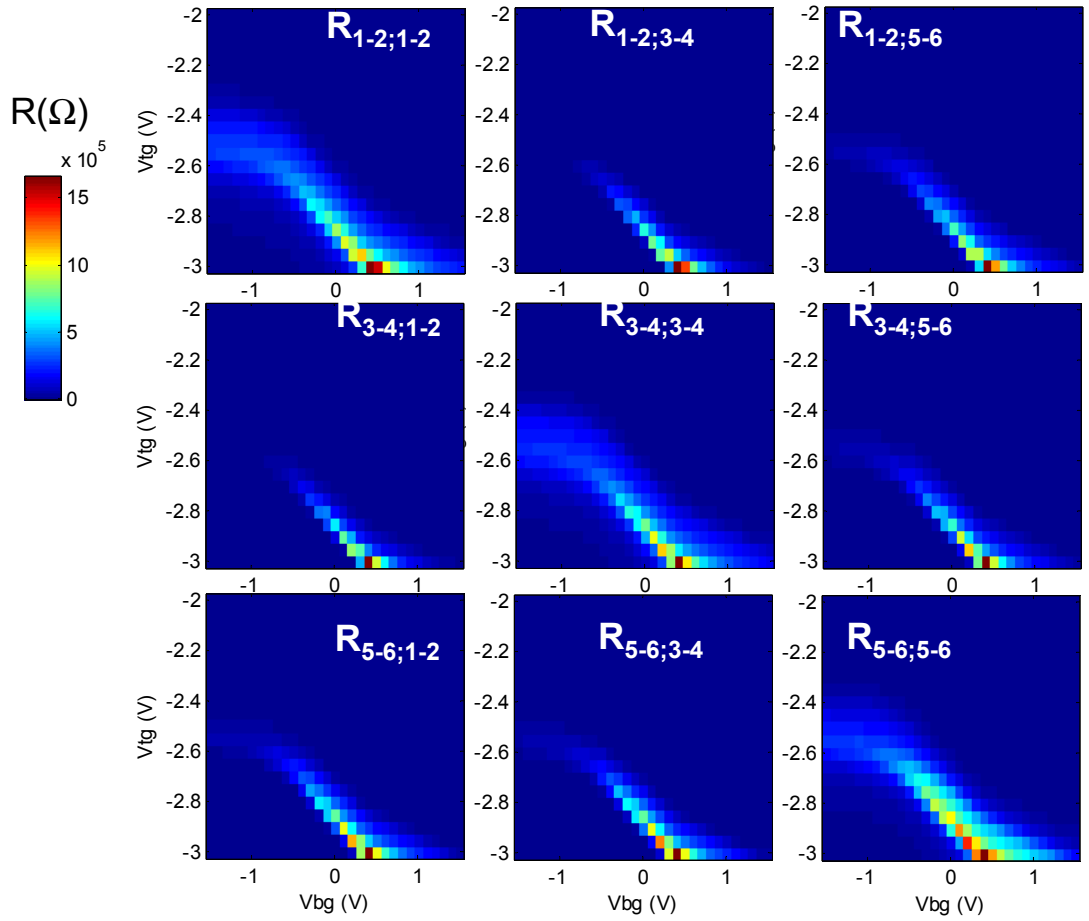

Figure S 6 Local and non-local resistance maps under different measurement configurations.

As a proof of edge conductance, Figure 2 in the main text already discussed non-local measurement with current running through leads 1-2 and voltage measured at leads 3-4 and 5-6. At the RP, voltages measured across 3-4 and across 5-6 are similar to the set voltage between 1-2. Same behavior is observed when current is running through the 3-4 pair or 5-6 pair and voltage measured across other pairs (*Figure S 6*). This clearly proves that the inner and outer edge are almost two equi-potential surfaces, a scenario only possible if there is substantial conductance along the edges.

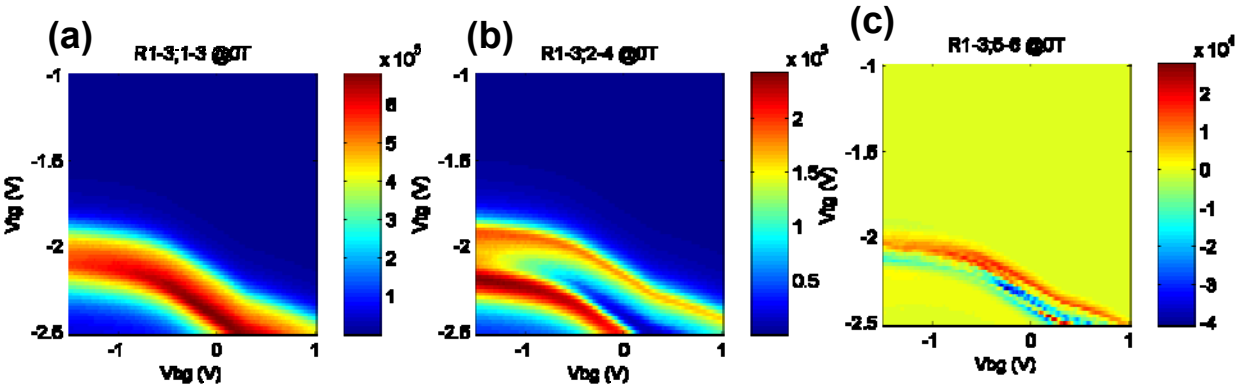

Figure S 7 Quasi local measurement in the Corbino ring device suggesting the presence of edge-conductance: (a) $R_{1\text{-}3;1\text{-}3}$, (b) $R_{1\text{-}3;2\text{-}4}$ and (c) $R_{1\text{-}3;5\text{-}6}$.

Evidence of edge conductance can also be seen from other quasi local measurement (e.g see *Figure S 7*). When current flows between 1-3, the discrepancy between local $R_{1\text{-}3;1\text{-}3}$ and quasi local $R_{1\text{-}3;2\text{-}4}$ delineates edge-dominated transport regime from bulk-dominated regime by the low resistance "tongue" in the middle of the resistance peak stripe of $R_{1\text{-}3;2\text{-}4}$. This is due to the electrical disconnection between 1 and 2, and between 3 and 4 when the bulk resistivity high, leads 2 and 4 become floating, resulting in low $R_{1\text{-}3;2\text{-}4}$. In addition, there is a substantial voltage built up between leads 5 and 6 at gate biases defining the resistance peak [*Figure S 7* (c)]. If the conductance is purely bulk-dominated, there should not be any built-up potential across 5-6, but it is not the case experimentally.

VI. Measurement at B=1T

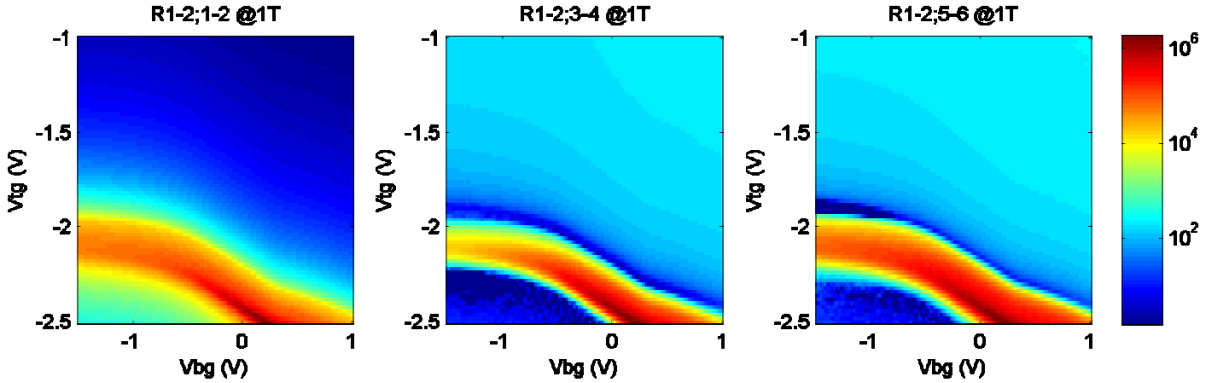

Figure S 8 Local and non-local resistance maps under B=1T.

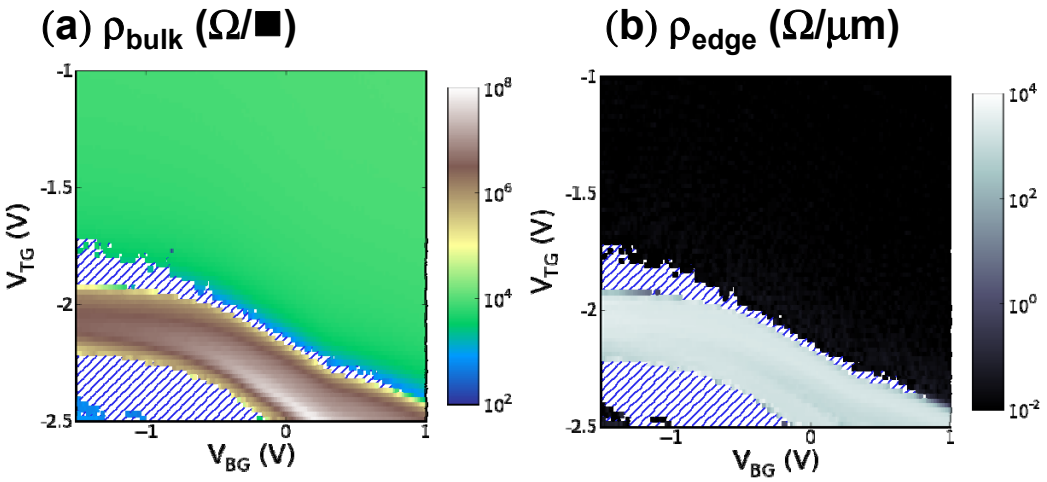

Figure S 9 Extracted bulk and edge resistivity at B=1T

Similar to analysis and extraction for B-0 and B=2T in the main text, additional data at B=1T are shown in *Figure S 8* and *Figure S 9* to illustrate the high dynamical range of the extraction technique. At B=1T, the ripplings are absent, but the increase of bulk resistance already allows for extraction of bulk and edge resistivity outside of the RP.

Reference

[1] Binh-Minh Nguyen, Wei Yi, Ramsey Noah, Jacob Thorp, and Marko Sokolich, Applied Physics Letters **106** (3), 032107 (2015).

[2] Fanming Qu, Arjan J. A. Beukman, Stevan Nadj-Perge, Michael Wimmer, Binh-Minh Nguyen, Wei Yi, Jacob Thorp, Marko Sokolich, Andrey A. Kiselev, Michael J. Manfra, Charles M. Marcus, and Leo P. Kouwenhoven, Physical Review Letters **115** (3), 036803 (2015).

[3] Lingjie Du, Ivan Knez, Gerard Sullivan, and Rui-Rui Du, Physical Review Letters **114** (9), 096802 (2015).

[4] M. J. Manfra, E. H. Hwang, S. Das Sarma, L. N. Pfeiffer, K. W. West, and A. M. Sergent, Physical Review Letters **99** (23), 236402 (2007).

[5] G. Chen, A. M. Hoang, S. Bogdanov, A. Haddadi, P. R. Bijjam, B.-M. Nguyen, and M. Razeghi, Applied Physics Letters **103** (3), 033512 (2013).